Rational SOFC material design: new advances and tools

Solid oxide fuel cells (SOFCs) offer great prospects for the most efficient and cost-effective utilization of a wide variety of fuels. However, their commercialization hinges on the rational design of low cost materials with exceptional functionalities. This article highlights some recent progress in probing and mapping surface species and incipient phases relevant to electrode reactions using *in situ* Raman spectroscopy, synchrotron based x-ray analysis, and multi-scale modeling of charge and mass transport. The combination of *in situ* characterization and multi-scale modeling is imperative to unraveling the mechanisms of chemical and energy transformation: a vital step for the rational design of next generation SOFC materials.

Meilin Liu[a,b]*, Matthew E. Lynch[a], Kevin Blinn[a], Faisal M. Alamgir[a], and YongMan Choi[a,c]

[a] *Center for Innovative Fuel Cell and Battery Technologies, School of Materials Science and Engineering, Georgia Institute of Technology, 771 Ferst Drive, Atlanta, GA 30332-0245, USA*

[b] *World Class University (WCU), UNIST, South Korea*

[c] *Current address: Chemistry Department, Brookhaven National Laboratory, Upton, NY 11973, USA*

**E-mail: meilin.liu@mse.gatech.edu*

The demand for clean, secure, and sustainable energy sources has stimulated great interest in fuel cells: devices that convert a chemical fuel directly to electricity. Among all types of fuel cell, solid oxide fuel cells (SOFCs) represent the cleanest, most efficient, and versatile energy conversion system[1], offering the prospect of efficient and cost effective utilization of hydrocarbon fuels, coal gas, biomass, and other renewable fuels[2,3]. However, SOFCs must be economically competitive to be commercially viable. An effective approach to cost reduction is to drastically reduce the operating temperature to 400 – 700 °C, thereby allowing the use of much less expensive materials in the components[4]. Unfortunately, lowering the operating temperature also lowers the fuel cell performance, as the electrode and electrolyte materials become less conductive and less catalytically active. Long term performance of SOFCs also degrades due to poisoning of the cathode by chromium from interconnect layers[5,6], deactivation of the conventional anode by carbon deposition[4-7] and poisoning by contaminants (e.g., sulfur) in the fuel gas[8-12].

One of the grand challenges facing the development of a new generation of low cost SOFCs is the creation of novel materials with unique compositions, structures, morphologies, and architectures that promote the fast transport of ionic and electronic defects, facilitate rapid surface electrochemical reactions, and enhance the tolerance to contaminants at low temperatures. In this article, we will highlight some

ISSN:1369 7021 © Elsevier Ltd 2011

recent progress, the remaining challenges, and future perspectives in the modeling, simulation, and *in situ* characterization of SOFC materials, in order to unravel the mechanism of electrode processes and ultimately achieve rational design of new materials and structures using a multi-scale computational framework rigorously validated by experiments at each scale.

Recent progress in materials development

The electrolyte

Oxygen ion (or vacancy), proton, and mixed ion conductors have been used for SOFCs (Fig. 1)[13]. As is well known, the advantages of SOFCs based on *oxygen ion conductors* include the formation of H_2O and CO_2 on the fuel side of the cell, which facilitates the use of carbon containing fuels through steam (H_2O) and dry (CO_2) reforming. However, the reaction products dilute the fuel. Although many candidate oxygen ion conductors have been studied[14,15], the materials that attract the most attention include doped zirconia, ceria, and $LaGaO_3$. For SOFCs based on *proton conductors*[14], the H_2O will form on the cathode side, diluting the air, not the fuel. Direct utilization of carbon-containing fuels is no longer possible with proton-conducting electrolytes. One prominent group of proton conductors is the $BaZr_{0.1}Ce_{0.7}Y_{0.2}O_{3-\delta}$ (BZCY) system[16], representing a good compromise between ionic conductivity and stability. It is also reported as a mixed ion conductor, allowing transport of both proton and oxygen ions. In particular, the $BaZr_{0.1}Ce_{0.7}Y_{0.2-x}Yb_xO_{3-\delta}$ (BZCYYb) system offers the highest ionic conductivity in the intermediate temperature range

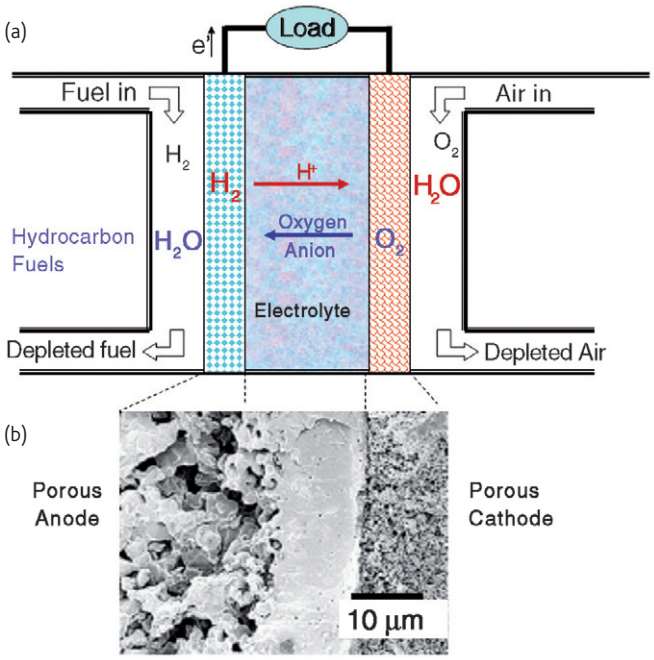

Fig. 1 (a) Schematic of an SOFC single cell based on proton and/or oxide ion conductors and (b) a cross-sectional view (SEM micrograph) of an SOFC single cell showing the typical microstructures of a dense electrolyte and porous electrodes.

and the ionic transference number may be tailored to some degree[2]. An ideal situation is to tailor the proton and oxygen ion transference number of the mixed ion conductor, allowing CO_2 to form on the fuel side while allowing most of the H_2O to form on the air side. Proton conductors have attracted considerable attention because of the low activation energy for proton conduction and thus high ionic conductivity at low temperatures. This class of mixed proton and oxygen ion conductors holds great potential for a new generation of low temperature SOFCs[2].

The air electrode (or cathode)

Cathode polarization still contributes considerably to energy loss in SOFC operation, more so at lower operating temperatures. The search for materials and architectures that are more active for oxygen reduction reactions (ORR) at lower temperatures has led to many candidate cathode materials[17], including doped $SrFeO_3$[18], $Ba_{0.5}Sr_{0.5}Co_{0.8}Fe_{0.2}O_{3-\delta}$ composites[19], and $Sr_{0.5}Sm_{0.5}CoO_{3-\delta}$ with a cone-shaped microstructure[20]. In particular, mixed ionic and electronic conductors (MIECs) have attracted attention because a high ambipolar conductivity may extend the active sites beyond the triple-phase boundaries (TPBs), thus offering better performance than a predominantly electronic conductor such as $La_{1-x}Sr_xMn\ O_{3-\delta}$ (LSM). To date, however, LSM-based composites (> 800 °C) and $La_{0.6}Sr_{0.4}Co_{0.2}Fe_{0.8}O_{3-\delta}$ (LSCF) (< 750 °C) still remain the most widely used cathodes for SOFC development; the adoption of alternative cathode materials is hindered by their unproven long-term stability and limited compatibility with electrolyte/other cell components, especially at high temperatures required for cell fabrication.

To counter this problem, many different types of catalytically active cathode materials have been infiltrated into the scaffolds of electrolytes (to form composite cathodes) followed by firing at a much lower temperature to avoid reactions between the electrolyte and electrode materials[21]. While it appears possible to make use of more active cathode materials and to show reasonable performance in small button cells using heavy coatings of Pt paste or mesh as a current collector, several critical issues still remain: the long-term stability of the cathodes is yet to be demonstrated due to degradation issues[21] and the poor conductivity for current collection could be much more severe in real cells or stacks where the use of Pt is no longer practical.

One reliable and effective approach is to modify the surface of the state-of-the-art cathode with a thin-film coating of a catalyst with higher stability and catalytic activity toward ORR. One example is a cathode consisting of a porous LSCF backbone and a thin coating of LSM[22]. The LSM-infiltrated LSCF allows the use of the best properties of two different materials: the excellent ambipolar conductivity of LSCF and the high stability and catalytic activity of LSM. The catalyst coating could be a *porous* layer of discrete particles or a *dense*, continuous film, as shown in Figs. 2a and 2b, respectively. Nanoparticles of ionic conductors such as

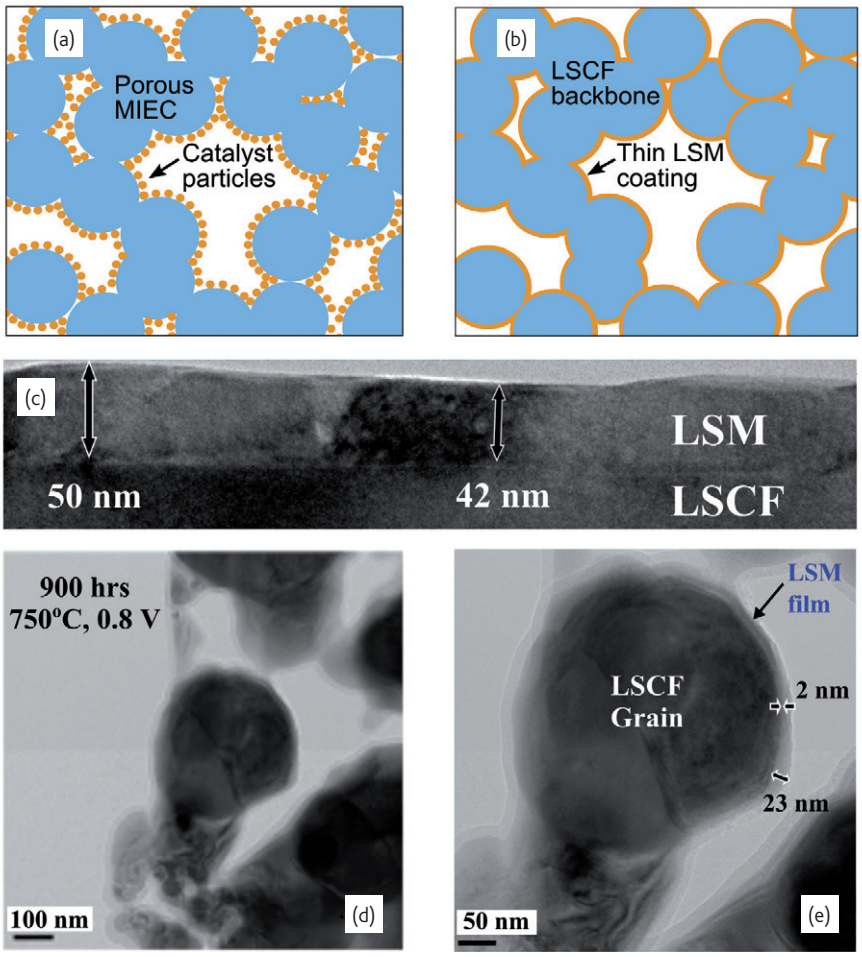

Fig. 2 A highly efficient cathode consists of an LSCF backbone having high ionic and electronic conductivity and (a) a porous layer of catalyst particles or (b) a dense thin film of catalyst having high stability and catalytic activity toward O_2 reduction (e.g., LSM), making effective use of the desirable properties of two different materials. (c) An LSM film (40 to 50 nm thick) on an LSCF substrate, (d) LSM infiltrated into a porous LSCF cathode (TEM image) after operation at 750 °C at 0.8 V for 900 hours, and (e) a closer view of the LSM coated LSCF grain in the LSM infiltrated LSCF cathode shown in (d). Parts b-e reprinted from[22] with permission of the Royal Society of Chemistry.

SDC have been successfully deposited on LSCF surfaces by the infiltration of aqueous nitrate solutions[23]. In contrast, dense films of LSM have been prepared using non-aqueous solutions[24], as shown in Figs. 2c-e. The challenges lie in how to achieve a rational design of the desired architecture and microstructure for each component, and how to fabricate a cathode with a reduced polarization and enhanced stability at low cost.

It is not always completely clear how to correlate the electrochemical performance *quantitatively* with the local structure, composition, and morphology of surfaces and interfaces of a cathode. Most approaches to electrode materials development tend to be very empirical in nature: a qualitative idea is developed, an electrode is fabricated, and a test is performed. The idea is considered a success if the performance meets or exceeds expectations. Part of the reason for the continued role of empiricism is the inability to establish the scientific basis for the rational design of better cathodes with enhanced stability and activity for oxygen reduction, which is a very hard problem. Nevertheless, rational design provides important insights into how to achieve higher cathode efficiencies through new architectures and new materials. Recent efforts in this direction are discussed later in this paper.

The fuel electrode (or anode)

Ni-YSZ cermet anodes are known to exhibit excellent performance in clean hydrogen or reformed fuels; however, Ni metal is susceptible to re-oxidation, carbon buildup (coking) in carbon-containing fuels, and deactivation by fuel contaminants (e.g., sulfur).

To overcome these critical technical barriers to fuel flexibility, a large number of "Ni-free" *alternative* anode materials have been developed; one prominent group of which is the conducting metal oxides, including $La_{0.75}Sr_{0.25}Cr_{0.5}Mn_{0.5}O_{3-\delta}$, (with a $Ce_{0.8}Gd_{0.2}O_{2-\delta}$ interlayer)[25], $Sr_2Mg_{1-x}Mn_xMoO_{6-\delta}$ ($0 \leq x \leq 1$)[26], and doped (La,Sr)(Ti)O_3[27,28]. Indeed, many alternative anode materials have shown much-improved tolerance to coking and contaminant poisoning; however, they have limited

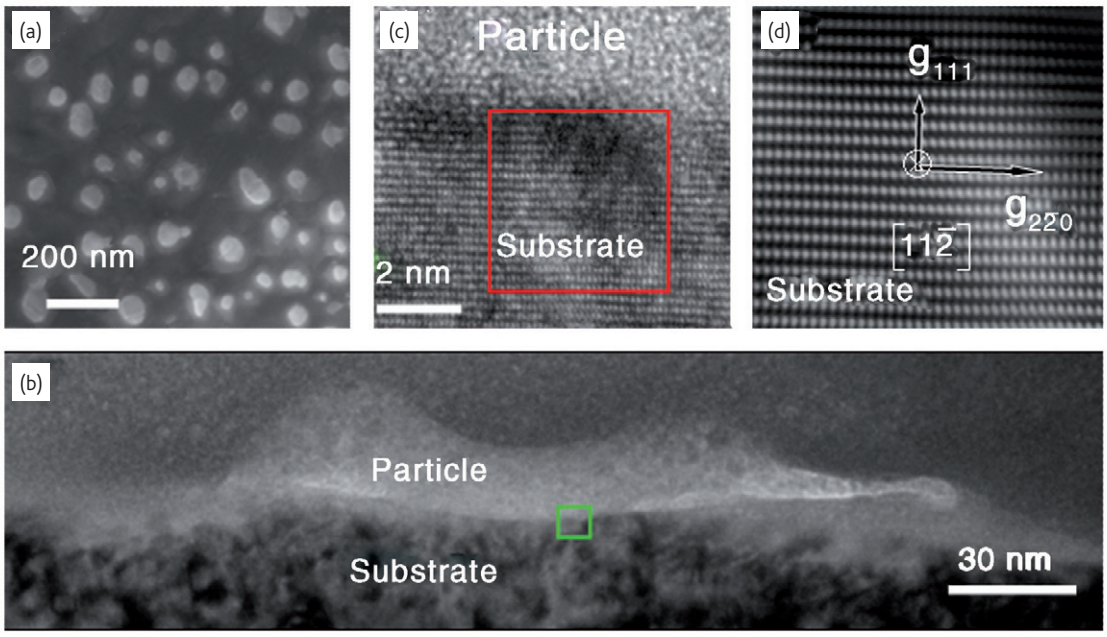

Fig. 3 Microanalysis of a BaO-modified Ni-YSZ anode: (a) top view (SEM image) showing the nano-islands of BaO on a Ni grain, (b) a cross-sectional view (bright-field TEM image) of a BaO/Ni interface, (c) HRTEM image of the BaO/Ni interface (the $[11\bar{2}]$ zone axis of the Ni under the BaO island is perpendicular to the page), and (d) Fourier-filtered $[11\bar{2}]$ zone axis image of the Ni under the BaO island. Adapted from[3] by permission from Macmillan Publishers Ltd: Nature Communications, ©2011.

physical, chemical, and thermal compatibility with the YSZ electrolyte during fabrication at high temperatures, which severely hinders their applicability to actual fuel cell systems.

Fabrication by *infiltration* of alternative electrode materials into a scaffold of electrolyte is perceived to offer advantages for improved structural stability and better thermal expansion matching. However, these claims are yet to be proven by experimental results.

Recently, a very different approach was adopted to achieve better sulfur tolerance: replacing the oxygen ion conductor YSZ in a Ni-YSZ cermet anode with a mixed-ion conductor like BZCYYb[2]; the -OH groups produced on anode surfaces by dissociative adsorption of water greatly facilitate oxidation of H_2S to SO_2 (thus removing sulfur from anode surfaces) and *in situ* reformation of carbon-containing fuels (thus minimizing coking) under typical SOFC operating conditions. This Ni-BZCYYb cermet anode showed superior sulfur tolerance at 750 °C for up to ~20 ppm H_2S using a cell based on a dense BZCYYb electrolyte and up to ~50 ppm H_2S using a cell based on Sm-doped ceria (SDC) dense electrolyte, suggesting that the critical pH_2S/pH_2 values are two to three orders of magnitude higher than that for a conventional Ni-YSZ cermet anode under similar conditions[10,29]. The sulfur tolerance exhibited is also significantly better than the Ni-YSZ anodes with YSZ replaced by other oxygen ion conductors of higher conductivity such as Gd-doped ceria (GDC) and Sc-stabilized zirconia (ScSZ)[30].

Among all anode materials ever studied, a composite anode consisting of Ni and the electrolyte still represents the state-of-the-art for anode-supported SOFCs because of the excellent catalytic activity for hydrogen oxidation, electrical conductivity for current collection, and compatibility with the electrolyte. One effective approach to making these composite anodes contaminant-tolerant is to modify the Ni-electrolyte surface by particles of catalysts that may promote the removal of contaminants (e.g., carbon or sulfur) while maintaining the unique properties of Ni required for high performance. As reported recently[3], small amounts of BaO spread over the surface of Ni grains in a Ni-BZCYYb cermet anode during processing at high temperatures may play a vital role in achieving the observed sulfur tolerance. In fact, when nano-sized BaO islands were created on the surface of the Ni grains in a Ni-YSZ cermet anode using a vapor phase deposition (Fig. 3), the resistance to coking was dramatically enhanced[3]. The nanostructured BaO/Ni interfaces seem very efficient for a water-mediated carbon removal. They also showed good sulfur tolerance while maintaining high performance.

Challenges in the rational design of materials

To date the development of new materials or structures has been guided largely by experience and chemical/physical intuition rather than by scientific theories or models, because the mechanisms of many charge and mass transport processes associated with fuel cell operation are still lacking. In this section we outline the main challenges we are facing in unraveling the mechanisms of electrode processes and the nature of the rate-limiting step, using both computational and experimental approaches, in order to control the rate of electrode processes or to achieve the rational design of better materials by changing the composition, structure, and morphology of materials.

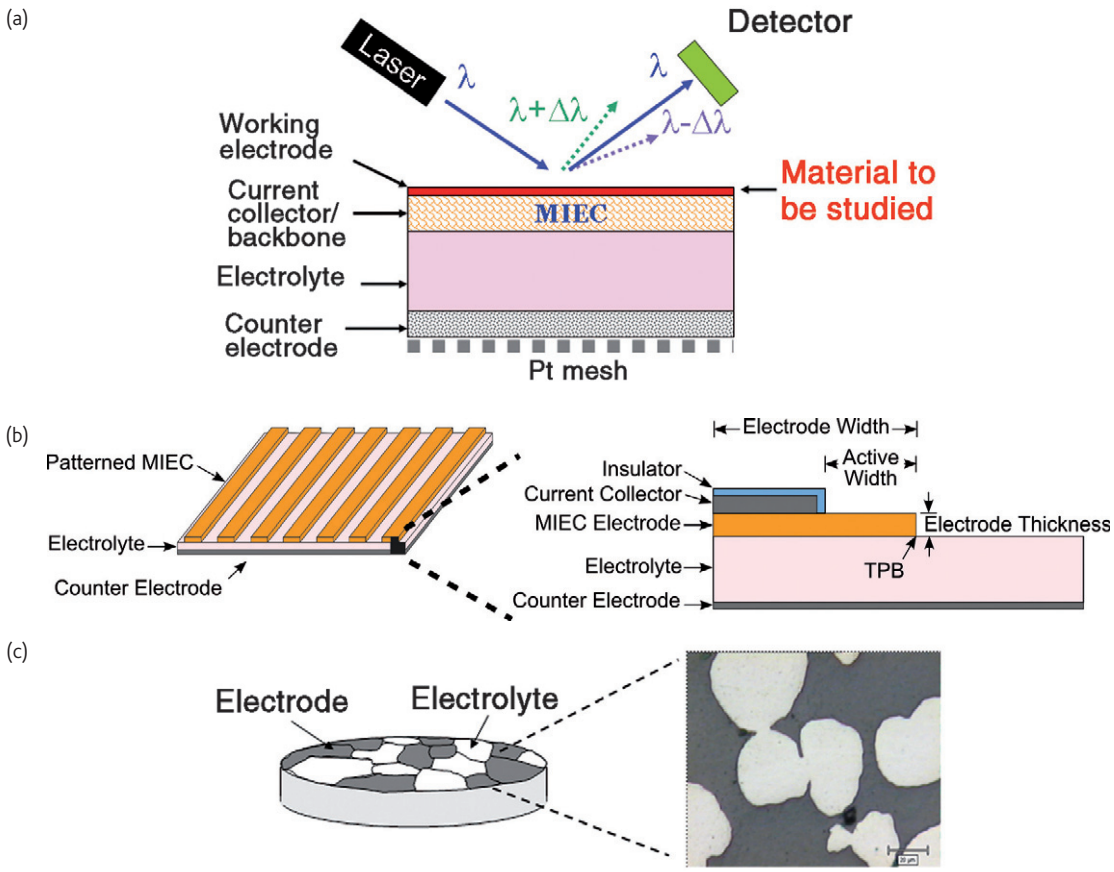

Fig. 4 (a) Schematic of a test cell with well controlled geometry: an MIEC film (current collector, the 2nd layer) coated with a dense film of a second cathode material (working electrode, the top layer), both deposited onto an electrolyte layer with a highly active counter electrode opposite. (b) A top and cross-sectional view of a test cell with a patterned electrode. Reproduced with permission from[33]. © 2008, The Electrochemical Society. (c) A schematic and an SEM image of a composite MIEC consisting of two phases (e.g., Ni-YSZ), which can be used as the current collector (as the 2nd layer) or be characterized (as the top layer) in the test cell.

Well-designed cells for electrochemical measurements

The rates of many chemical and energy transformation processes are limited by the charge and mass transfer along surfaces and across interfaces. A fundamental understanding of these processes, especially the rate-limiting step, is vital to enhancing electrode performance.

Electrochemical measurement is an effective technique for quantifying the performance of a cell or a cell component, offering phenomenological parameters such as charge or mass transfer resistance or area specific resistance (ASR), exchange current density, and transference numbers. These parameters are helpful when predicting performance using continuum models. However, they may not represent the intrinsic catalytic properties of an electrode material because they may be influenced by many factors which are difficult to control experimentally, including the geometry, microstructure, and transport properties of the electrode as well as its physical and chemical compatibility with the electrolyte.

To preclude the effect of extrinsic factors (e.g., geometry and microstructure), a test cell *platform* with well-controlled geometry must be used[31]. One example is a dense or patterned film electrode of the material to be examined, which functions as the working electrode, as schematically shown in Figs. 4a and b, respectively[22]. The secondary current collection layer, the MIEC layer in Fig. 4a, is sufficiently thick to alleviate sheet resistance and therefore does not require a densely packed metal current collector, allowing exposure of the working electrode surface for other *in situ* characterization. This cell is ideally suited for characterization of the intrinsic properties of an electrode material (the top layer), which is also open to other *in situ* characterization such as Raman spectroscopy and scanning probe microscopy. When dense, the working electrode material must have some degree of mixed conductivity (poor ionic conductivity may be mitigated by reducing the thickness). To minimize the sheet resistance effect of a thin-film electrode, an MIEC of high ambipolar conductivity has to be used as the current collector, which can be a homogenous (like LSCF) or a composite (like YSZ-LSM or Ni-YSZ, Fig. 4c) MIEC. Another advantage of this cell design is that only the top surface is active for electrochemical reactions, which is open to other simultaneous *in situ* measurements such as Raman spectroscopy or x-ray analysis due to the underlying current collection layer and,

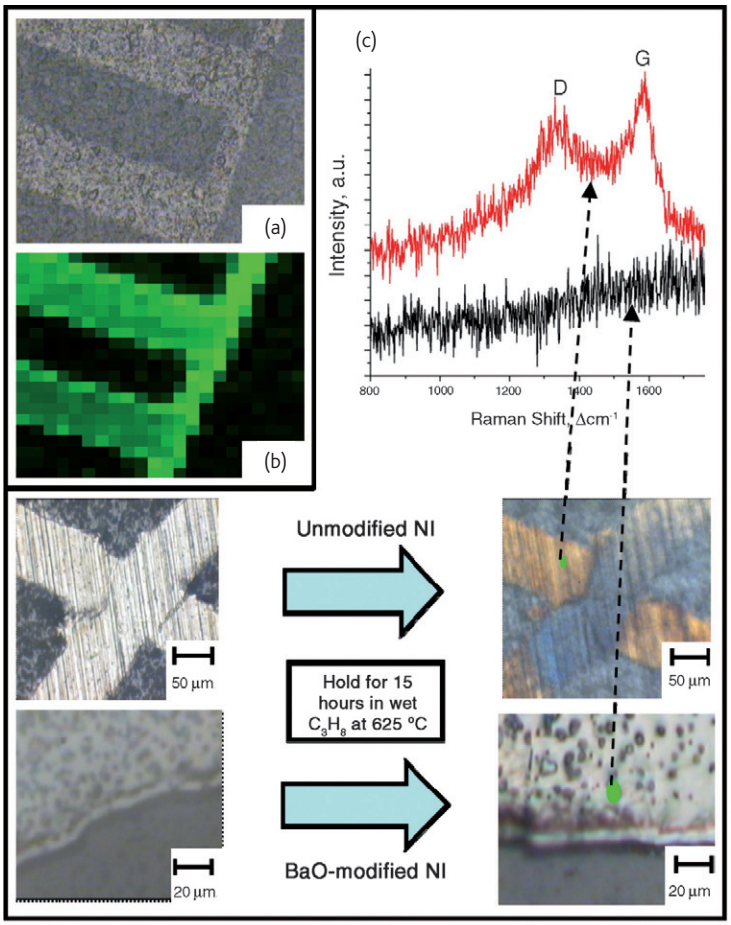

Fig. 5 (a) Optical micrograph of a patterned Ni electrode (lighter area) on YSZ after exposure to CH_4 at 625 °C for 12h. (b) Raman intensity map for a 1580 cm^{-1} Raman shift (carbon G-band) of the same area shown in (a). The detailed experimental arrangement for the Raman measurement is described elsewhere[10]. (c) Comparison of coking behavior between bare a Ni mesh electrode and BaO-modified electrode using Raman spectromicroscopy.

therefore, lack of interference by bulky metal mesh or even metal paste.

To further isolate certain charge or mass transfer step(s) of the electrode reactions, continuum models have been developed for the careful design of cell geometry (e.g., the thickness of MIEC film) to minimize the sheet-resistance effect in the thin-film working electrodes[32]. Models have also been developed for the design of cells with patterned electrodes for direct correlation between performance and electrode geometry (e.g., thickness, TPB length) to minimize experimental errors[33]. These cell designs are instrumental for the reliable determination of the intrinsic properties of electrode materials.

The use of well-designed cells is vital for the collection of useful information, since the interpretation of data becomes difficult for cells with complicated porous electrodes. For example, while it is possible to achieve *satisfactory* or even *perfect* curve fitting to impedance data involving intricate charge and mass transfer processes with similar relaxation time constants, there is no way of knowing if the assumed number of processes adequately reflects what is occurring in the cell, if the proposed equivalent circuits are meaningful, or if the assigned values for circuit elements are valid, let alone the errors associated with the de-convolution of the overlapping data. When complications occur in data interpretation, the best solution is to *simplify* the cell for electrochemical measurements by isolating the response from a cell component or separating charge from mass transfer, as discussed earlier. It is noted, however, that some difference may exist between bulk properties of a porous material and those of the material as a thin film[34,35]. Careful validation is necessary to make well designed test cells a valuable tool for the evaluation of fundamental electrode properties.

However, an *electrochemical* measurement cannot provide direct information for identifying the chemical species involved in electrode reactions or changes in electrode materials under the test conditions. *In situ* characterization techniques can be performed alongside electrochemical measurements, including Raman spectroscopy and AFM (see Fig. 4a). Probing and mapping the evolution of surface composition and structure or incipient new phase formation on electrode surfaces relevant to electrode reactions under practical fuel cell operating conditions may provide critical insights into the

mechanisms of these reactions, which are vital to achieving rational design of better electrodes, catalysts, and interfaces.

In situ Raman spectroscopy

Since a number of chemical and electrochemical reactions limit SOFC performance, a detailed knowledge of the surface species involved in those processes is vital to the design of new SOFC materials and microstructures. Among the relatively few *in situ* surface analysis methods (FTIR, Raman, EXAFS, and small-angle x-ray scattering)[36], Raman spectroscopy is the most flexible in terms of having the largest window of operating conditions and the greatest range of surface species that can be probed and mapped, especially oxygen[37,38], sulfur[10,39,40], carbon[9,41,42], hydrocarbons[43], and water[2,3]. Raman spectroscopy can be used *in situ* (and *ex situ*) alongside electrochemical measurements to probe and map surface species (e.g., reaction intermediates) and chemical phases relevant to the electrode reactions under practical fuel cell operating conditions, allowing the direct correlation of electrochemical performance to surface chemistry and structure in the electrochemical environment of an operating cell. A typical arrangement for in situ Raman analysis of SOFC electrode materials is described elsewhere[10].

A multitude of research efforts in recent years have led to marked progress in the development of Raman spectroscopy as an effective tool for studying SOFC materials, including the investigation of sulfur poisoning on Ni-based anodes[39,40], chromium poisoning of LSM cathodes in cells with metallic interconnects[6], and the oxidation state of GDC electrolytes under fuel cell atmospheres[44]. Studies of coking on SOFC anodes operating on carbon-containing fuels have garnered attention from researchers in this area due to the reasonable sensitivity of Raman spectroscopy to carbon species[9,41,42,45-47]. Walker's group was the first to develop and demonstrate a Raman microscope system for *in situ* studies of coking on Ni-YSZ anodes[45], and this methodology was adapted for similar investigations by others[42,46,47].

More recently, efforts have been devoted towards vastly improving spatial resolution in these types of studies[41]. For example, Fig. 5a shows an optical image of a patterned Ni strip electrode deposited by PVD on YSZ that was exposed to CH_4 at 625 °C for 12 hours, while Fig. 5b shows an intensity map of the same area for a 1580 cm^{-1} Raman shift, corresponding to the carbon G-band. The intensity map very clearly resolves the Ni electrode, on which the coking should preferentially occur. Additionally, Raman spectromicroscopy has been used to characterize coking resistance conveyed by surface modifications to Ni electrodes. Fig. 5c shows a comparison of coking behavior between a plain Ni mesh electrode and one that has been modified with BaO (see above), the latter of which shows no coking even after 16 hours of exposure to C_3H_8 at 625 °C under OCV conditions due to BaO islands on the surface, of which clusters are visible in the micrograph. The spectra shown were collected *in situ* under treatment conditions.

In the future, Raman spectroscopy will provide critical insights into the pathway, sequence, and mechanism of reactions occurring on SOFC electrode surfaces under electrochemically polarized conditions. The presence of specific chemical species on electrode surfaces will be correlated with impedance spectroscopy data under various operating conditions to understand how different species impact fuel cell performance. A profound understanding of the detailed electrode reaction mechanism and knowing which step affects cell performance the most will guide the development of new electrode materials and microstructures.

While Raman spectroscopy has been successfully used to probe and map carbon, sulfur, Cr-containing phases, water, and oxygen species, many challenges still remain in pin-pointing important reaction mechanisms relevant to fuel cell operation. These obstacles include a lack of sensitivity for probing and mapping the *earliest stages* of phase formation related to coking and sulfur poisoning as well as the limited amount of signal from oxygen species on cathode surfaces, due to the small Raman cross-sections of those species. In particular, for common cathode materials like LSM and LSCF, a high tendency for fluorescence necessitates the use of a lower excitation power, diminishing the useful Raman signal. Additionally, the high temperatures associated with *in situ* testing further decrease the sensitivity and may lead to a shifting of the characteristic Raman bands. To overcome these difficulties, surface-enhanced Raman scattering (SERS) methods applicable to SOFC materials are being developed to increase sensitivity[48]. In addition, Raman spectroscopy integrated with scanning probe methods, which can allow for tip-enhanced Raman spectroscopy (TERS) can potentially increase both sensitivity and spatial resolution[49].

In situ synchrotron-based XRD/XAS

Synchrotron-based x-ray techniques provide yet another methodology for *in situ* investigations of SOFC materials. When acting as *in situ*

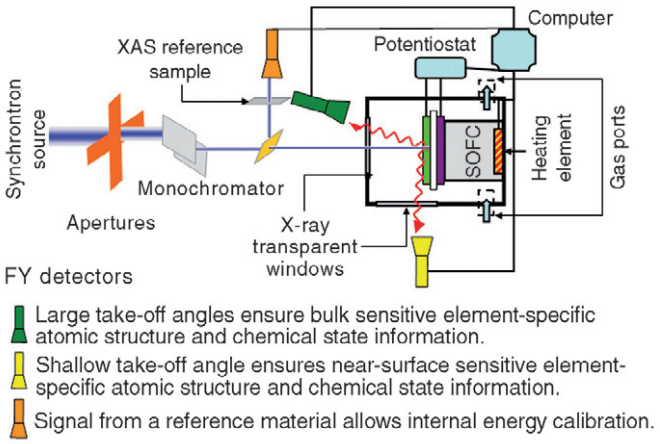

Fig. 6 A schematic arrangement for an in situ synchrotron-based XAS study of SOFC materials under conditions similar to fuel cell operation alongside electrochemical measurements.

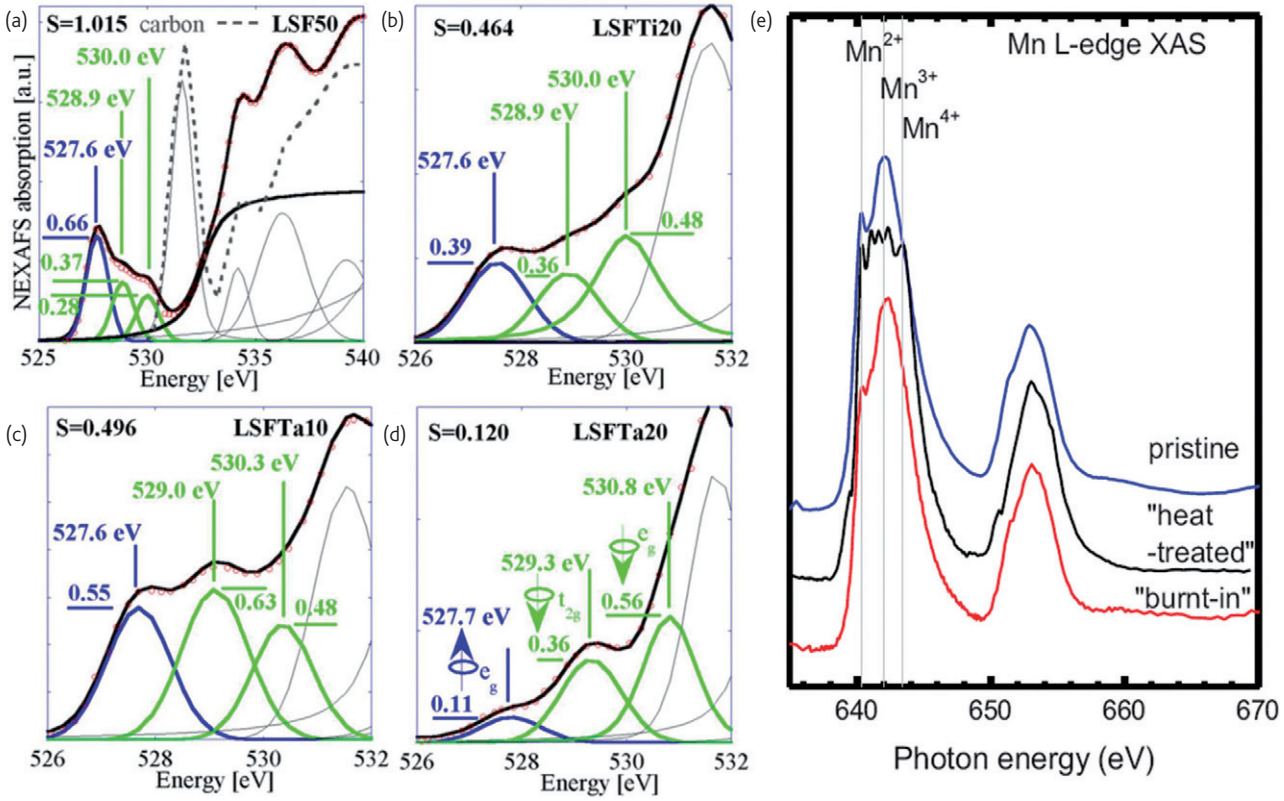

Fig. 7 (a-d) Deconvoluted oxygen 1s spectra with a pre-peak near EF for LSF and LSF doped with Ti (20 mol.%) and Ta (10 and 20 mol.%). Numerals indicate peak position and spectral weight. Reproduced from[50] with permission of the American Institute of Physics. (e) Mn L_3-edge XAS of LSM as-processed (blue), SOFC environment exposed (black), and activated (red) films. The Mn charge-state multiplet line shape peak energies are plotted as vertical lines. Reproduced with permission from[51]. © 2011, The Electrochemical Society.

structure probes for SOFC materials, x-ray absorption spectroscopy (XAS) is excellent in probing the local atomistic and electronic structure, as shown schematically in Fig. 6, while x-ray diffraction (XRD) is a powerful tool for eliciting lattice or long-range order. Often, the structures of SOFC materials may change due to a chemical, electrochemical, and/or thermal effect under typical operating conditions. The atom specificity of XAS makes the technique very powerful for characterizing electrode reaction mechanisms. Since the near-edge structure of XAS data (XANES) probes the chemical state of a particular elemental component while the extended fine structure (EXAFS) describes its local atomic environment, combining XANES and EXAFS of multiple atomic species over an SOFC reaction can be used to create a reaction roadmap. At the same time, XRD can identify the crystalline phases involved in the reactions and draw out the phase transformation windows in temperature, $P_{O2,}$ or other external stimuli.

XAS can be performed in multiple modes simultaneously, barring constraints of sample geometry and sample chamber pressure and temperature. Transmission mode XAS measurements at hard x-ray energies are forgiving experiments to set up under *in situ* conditions and provide access to the K-edges of *3d* transition metals, Sr, and Y, and the L_3-edges of Ba, La, and Ta. Fluorescence yield (FY) measurements here are particularly useful when the element being probed is a dilute component of the material (e.g., the dopants). Near-surface electronic structure measurements, using total or partial electron yield (TEY/PEY), can be made simultaneously with corresponding bulk measurements using fluorescence yield (FY) or direct transmission, and provide contrast between surface and bulk phenomena. As described earlier, XANES provides the chemical state of a species, but to be more specific, it provides a spectral function that is proportional to the unoccupied densities of state local to that species. In the commonly found transition metals with octahedral symmetry in SOFC materials, for example, the oxygen K-edge or the metal L-edge will show the split t_{2g} and e_g LUMO orbitals (provided they have empty states). Fig. 7 shows the deconvoluted oxygen K-edge (transition between the oxygen *1s* initial state and LUMO final states with *p*-symmetry) in LSF with and without Ti and Ta doping[50]. After deconvoluting the oxygen K-edge prepeaks into individual t_{2g} and e_g spin up and spin down bands, Braun *et al*. discovered a correlation between a ratio of peak heights, the conductivity, and the Fe^{4+} /Fe^{3+} ratio. Also shown in Fig. 7 is the Mn L-edge data (Mn *2p* electrons excited to Mn *3d* final states) in LSM, clearly showing the contributions of three types of Mn ion[51].

Transmission *in situ* XAS can be carried out in a proper furnace at reaction temperature and P_{O2} like the one at beamline X18B of the National Synchrotron Light Source where multiple samples can be placed in a carousel and exposed to the same reaction conditions. An example of *in situ* XANES of SOFCs can be seen in the work of Yildiz and co-workers who studied the activation of $La_{0.8}Sr_{0.2}MnO_3$ and $La_{0.8}Ca_{0.2}MnO_3$ on single crystal YSZ electrolytes using *in situ* XANES (Mn K-edge and La L_2-edge and x-ray reflectivity)[52]. For enhanced surface sensitivity under *in situ* conditions, a grazing incidence FY geometry can be used, such as the one demonstrated by Shinoda *et al.*[53].

There are currently a handful of examples for the use of *in situ* XRD for structural characterization of SOFC materials. Liu *et al.* studied phase and strain distributions associated with reactive contaminants in SOFCs[54]. Using *in situ* measurements, Shultz *et al.* characterized the dissociation and crystallization of the amorphous precursor powders of lanthanum strontium gallates[55]. More recently, Hashimoto *et al.* investigated the changes in the lattice parameters of $La_{0.6}Sr_{0.4}Co_{1-y}Fe_yO_{3-\delta}$ (y = 0.2, 0.4, 0.6, and 0.8)[56]. Further, a combination of both XAS and XRD would be a very powerful approach to probing local and long-range atomistic structures of SOFC materials under practical fuel cell operating conditions, offering structural information that has never before been accessible.

Prediction of intrinsic properties of materials

Proper modeling techniques and prediction tools are essential to a comprehensive understanding of SOFC materials. For example, density functional theory (DFT)[57] is an effective computational framework for prediction of electronic structures and other fundamental properties of materials[58-60]. In particular, it has provided detailed, molecular-level information that may not be readily obtained experimentally, including probable electrode reaction sequence, mechanisms, and stable intermediates, surface coverage of adsorption sites, mobility of electro-active species along surfaces, and rate constants for adsorption/dissociation, reduction/oxidation, and incorporation/release of species at surface sites. For example, the significance of the MnO_2-terminated (001) surface of $LaMnO_3$ was reported[61] and, in conjunction with molecular dynamics (MD) simulations[62] and kinetic theory[63], several properties of $LaMnO_3$-based materials were examined for SOFC applications[62-64] including reaction sequences and charge transfer mechanism. Recently, an *ab initio* thermodynamic approach was used to examine oxygen reduction on SOFC cathodes.[65,66] Fig. 8 depicts a molecular-level computational screening based on surface and bulk properties to search for cathode materials of higher performance than conventional ones[67]. DFT calculations were also used to design sulfur- and carbon-tolerant anode materials[59,68-70]. The interactions of sulfur-containing compounds (e.g., H_2S) with anode materials under SOFC operating conditions were predicted using *ab initio* thermodynamics[12]; providing important insights into the mechanism of sulfur poisoning.

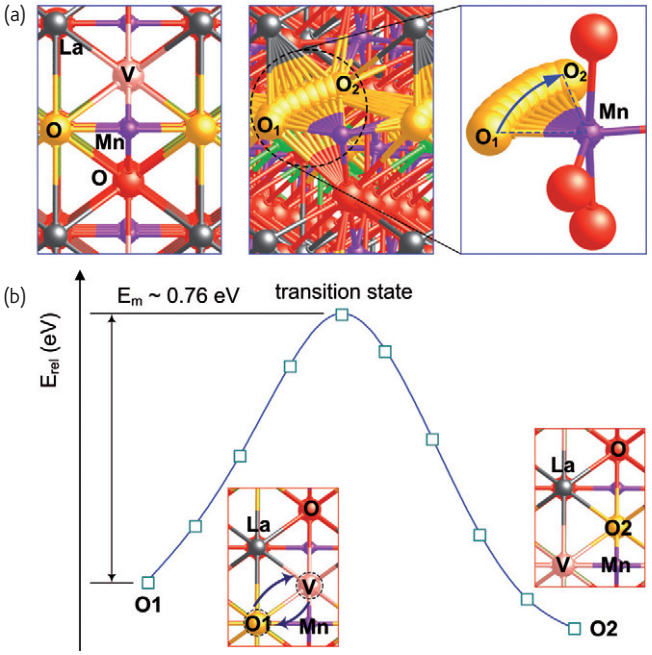

Fig. 8 (a) Illustration of a bulk $La_{0.5}Sr_{0.5}MnO_{2.75}$ (110) structure before and after ionic conduction. V and O_N (N = 1 or 2) are, respectively, an oxygen vacancy and the nearest neighboring oxygen to V. (b) Trajectory of oxygen ion conduction through $La_{0.5}Sr_{0.5}MnO_{2.75}$ (110). O1 and O2 are the initial and final states of the oxygen ion conduction. Reprinted from[67] with permission from Elsevier, © 2011.

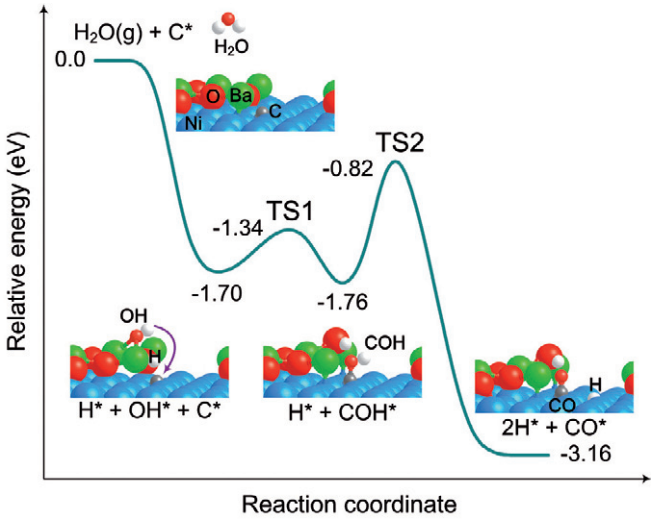

*Fig. 9 DFT-predicted energy profile for removing chemisorbed carbon species on BaO/Ni(111) interfaces through a water mediated process, where * denotes an adsorbed species on the surface. Adapted from[3] by permission from Macmillan Publishers Ltd, © 2011.*

Recently, a water-mediated removal of carbon species from nano-structured BaO/Ni interfaces was modeled successfully (Fig. 9)[3]. Furthermore, the predicted vibrational frequencies of surface species and new phases were confirmed using Raman spectroscopy[71].

While DFT-based calculations have been instrumental in gaining critical insights into intrinsic properties of many materials[72], new methodologies must be developed to bridge the gap between theoretical predictions and experimental measurements, notably for the materials with open shells of *d* or *f* electrons commonly encountered in SOFC systems[60,73]. For example, the DFT+U theory has been proposed to mitigate the limitations of conventional DFT for these materials. Further, time-dependant DFT[60] has also been applied to the analyses of x-ray absorption spectra of SOFC materials.

On the other hand, DFT calculations become increasingly more difficult for more complex material systems, such as the BZCYYb electrolyte, the LSCF cathode, and LSTC anode materials, due partially to the large number of atoms/ions (or potential reactive sites) that must be considered in the calculations. It is still a grand challenge to identify *approximate descriptors* for the computational design of better SOFC materials, something similar to the *d* band model applied to the characterization of the oxygen reduction reactions (ORR) in low temperature fuel cells. Moreover, electrochemical hot spots, such as the heterogeneous boundaries and junctures in a porous electrode (e.g., TPB), are even more difficult to predict using DFT-based calculations. The quantum mechanics/molecular mechanics (QM/MM) methodology[74] may help model reactions at or near the TPB region.

To link the intrinsic properties of a material with its performance in a fuel cell, however, DFT/MD simulations must be combined with continuum modeling that can predict the phenomenological behavior of materials, which can be confirmed directly by experiments.

Continuum modeling

Coupled continuum and phenomenological models can be used to predict experimentally measurable parameters, such as exchange current density and ASR of a cell, providing a means to evaluate response over larger length scales than those available to DFT/MD simulations. Phenomenological models provide a means to understand the rates of charge and mass transfer processes in detail and predict them in a variety of circumstances. The rate expressions serve as boundary conditions for continuum models. Fig. 10 illustrates the interdependence of models at different length and time scales (from DFT to continuum) for the rational study of SOFC materials.

Once phenomenological parameters are known, these models in turn can predict the behavior of materials or the performance of fuel cells under various conditions. For example, continuum models have been successfully applied to various aspects of electrode operation[75], from the global response of porous mixed conducting electrodes[76,77], to the performance of heterogeneous composite electrodes described using particle/resistor networks[78] and homogenized treatment[79], and to detailed reaction rates or intermediate steps of surface and interfacial processes[80].

Further, continuum models can link DFT/MD calculations indirectly to experimental measurements, thus providing a means of verifying their predictions. For example, continuum models can be used to predict performance of fuel cells from materials properties derived from DFT/MD simulations, including the molecular level reaction sequence, rate-limiting steps, detailed defect structures, surface structures, and phenomenological parameters (e.g., surface adsorbed oxygen concentration[73]), some of which may not be readily accessible from experiments. Phenomenological/continuum models guided by DFT/MD can then be compared to experimental results to verify and/or refine these calculations.

Moreover, phenomenological/continuum models *conformal to electrode geometry* have been successfully used with cells consisting of thin-film/patterned electrodes. On the simplest level, they help to quantify the characteristic activity under the framework of linearized parameters, such as the length-normalized resistance to oxygen reduction at the TPB[81] or the area-normalized equivalent circuit parameters of the bulk pathway[82]. A model conformal to electrode geometry is required to examine the effect of the microstructure on the performance of a porous electrode. Conformal models have been successfully coupled with phenomenological models to explain[83] and help mitigate[32] sheet resistance observed in experimental patterned electrode results, thus providing guidelines for the better design of test cells and for the proper interpretation of electrochemical measurements[84]. As described in detail elsewhere[32,33], these models have been used to predict potential and defect distribution in a thin-film working electrode with current collectors of different geometries (strips, grids, and circular pads), the critical spacing between current collectors to minimize the effect of sheet resistance on performance, and the relative contributions from competing bulk and TPB pathways of a patterned electrode under cathodic polarization. Recently, phenomenological modeling was used together with DFT simulation predictions and TEM analysis to examine the trend of the ASR of uncoated and LSM-coated LSCF electrodes under various cathodic polarizations[22].

The reactions on both cathode and anode are quite complex, often involving adsorption, dissociation, and reduction/oxidation of gas molecules, transport of adsorbed surface species, and participation of point defects (e.g., oxygen vacancies and electrons/electron holes). An electrochemical driving force may not only alter the concentrations of surface species within a mixed conductor but also change their energies[85]. Further, the composition and structure of an active electrode surface may be different from those of the bulk phase due to surface elemental segregation[86]. The linking of electrochemical response with detailed surface properties and reaction mechanisms, therefore, is quite a challenge and continues to be an important research pursuit.

Quantification of the microstructure effect

The performance of an electrode is determined critically by the porous 3D microstructure. Important factors include the exposed catalyst

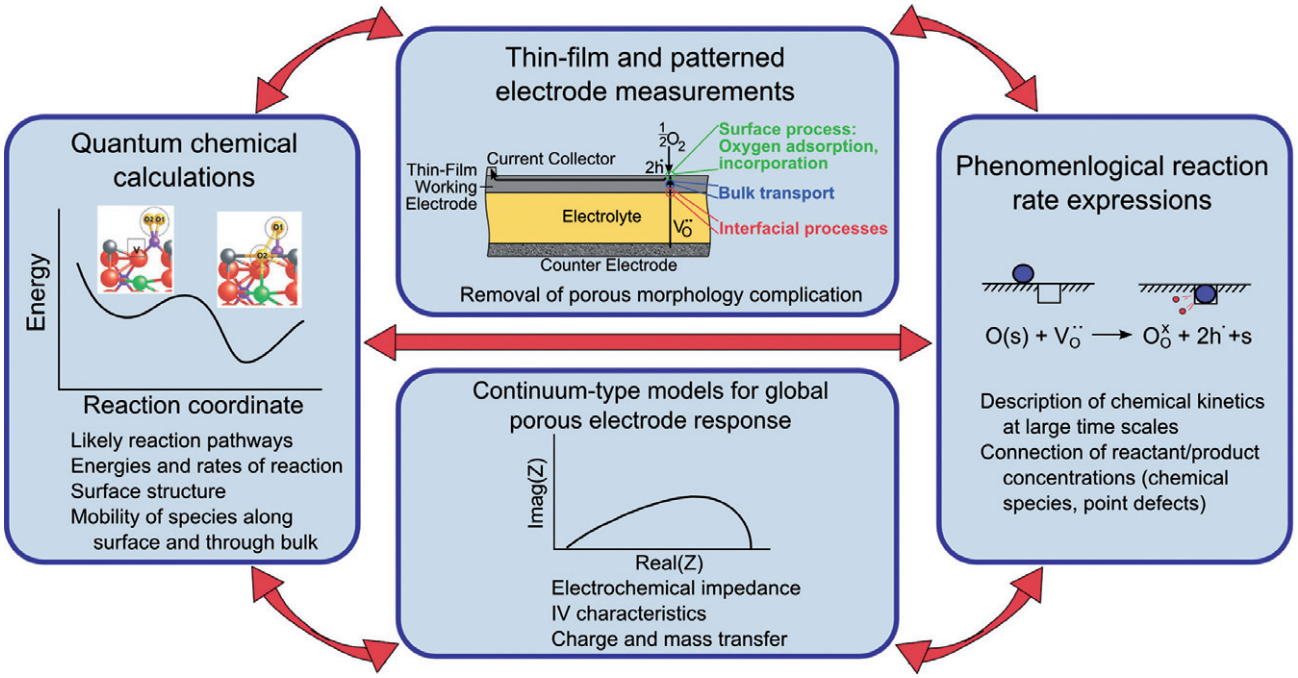

Fig. 10 Interdependence of models at different length and time scale and characterization techniques for the rational study and design of SOFC materials.

surface area, facility of gas transport through pores, resistance to ionic and electronic transport through solid phase, and length of TPB lines. The complexity of mass and charge transport in just the solid phase is illustrated in Figs. 11a,b. Many strategies have been employed to optimize the microstructure, including the formation of composite electrodes, functionally graded microstructures, and infiltration of active electrode phases on electrolyte scaffolds. Optimization of the electrodes is a very difficult task because many of the important features compete with one another; for example, surface area may increase at the expense of gas-phase diffusion.

Modeling on an electrode level[75,87] is useful for understanding performance. In particular, equivalent circuit models[78,88] describe the performance based upon linearized parameters. Another model type for mixed ionic-electronic conducting electrodes is based upon porous electrode theory[76] and uses homogenized microstructural parameters and linear irreversible thermodynamics in reaction rates. Recent results show that it is reasonable for many MIECs, but not for those where diffusion length is on the order of particle size[89], because they neglect the fine details of the microstructure and can lack detailed predictive capability.

3D reconstruction by FIB/SEM[90,91] and phase-sensitive x-ray computed tomography[92] is a recent and promising development, providing high-resolution microstructural details of porous electrodes. This information has been used in homogenized models for performance prediction.

Recently, researchers also began to use the 3D reconstructions as the domain for electrochemical simulations using the Lattice-Boltzmann method[93,94] or the finite element method[95]. The former has been applied primarily in the anode using models developed for nickel patterned electrodes, gas diffusion, and ionic transport. The latter has been applied to an LSCF cathode using effective linear irreversible thermodynamic parameters (not detailed reaction rates) based on surface exchange and tracer diffusion coefficients. We have developed FEM models for the simulation of the electrochemical response of 3D porous electrodes reconstructed by x-ray computed tomography[92]; the preliminary results are shown in Fig. 11c.[96]

While simulations conformal to the reconstructed electrode microstructures constitute a powerful computational framework, some challenges still remain. First, the 3D reconstructions may require extensive and skilled FIB/SEM or synchrotron work. Second, simulations deployed on the actual porous structures require sophisticated numerical methods and, depending on the complexity of phenomena modeled, can require complicated constitutive equations and/or parameter determination. All are the subject of current research within the field.

Such simulations can corroborate the accuracy of homogenized models and, when homogenized models break down, provide the most accurate and detailed means of simulation. The detailed microstructure may also be able to act as a sort of well-defined electrode in and of itself: the *a priori* digital representation of explicit microstructural geometry might allow fundamental study. The ultimate goal is to use the 3D geometry for numerical simulation of electrode performance in engineering design, in conjunction with

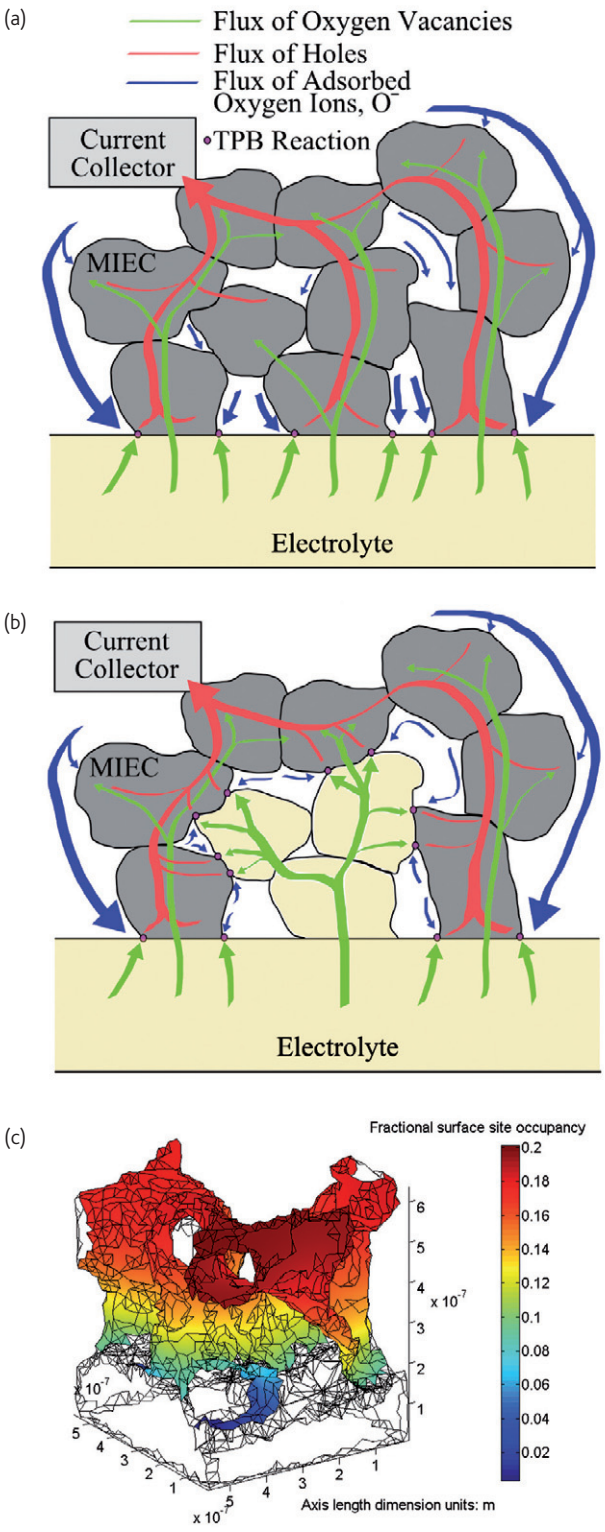

Fig. 11 Schematic diagram of charge and mass transport within and on the surface of (a) a single-phase mixed conducting porous electrode and (b) a composite (mixed conductor + electrolyte) porous electrode. (c) Initial 3D FEM simulation of adsorbed oxygen species on the surface and at the TPBs of a porous LSM electrode[96].

detailed, mechanistic, nonlinear phenomenological rate expressions serving as boundary conditions[97] and informed by parameters derived from patterned or porous electrodes.

New directions and future perspectives

One important direction is to exploit nanostructures and nano-architectures derived from a variety of templates in order to transcend some of the difficulties facing materials development for energy applications[98]. In particular, hierarchical 3D porous architectures[99] may dramatically enhance the rates of change and mass transfer processes while improving the mechanical integrity and robustness. These nanostructured electrodes and interfaces are known for increased numbers of active sites, reduced length of ion diffusion to active sites, and greater flexibility in surface modification for catalysis and electro-catalysis[98,100].

Another important new direction is to develop a predictive multi-scale (from DFT to continuum) computational framework, through rigorous validation at each scale by carefully designed experiments under *in situ* conditions, for the rational design of better materials and structures for a new generation of SOFCs to be powered by readily available fuels. While significant progress has been made in developing SOFC materials in probing and mapping electrode surface species relevant to electrode processes, and in unraveling some of the mechanisms of the electrode processes, many challenges still remain to bridge the gaps between models at different scales or between theoretical predictions and experimental observations[10]. Only when the detailed mechanisms of the rate-limiting steps are clearly understood will it be possible to rationally design better materials.

It is vital to perform well designed experiments at each scale under *in situ* conditions in order to validate and perfect the predictability of the individual models at different scales. It is still a grand challenge to link the *global* performance or functionality of a 3D porous electrode with the *local* structure, composition, and morphology of nanostructured surfaces and interfaces. Validation and integration of information collected from different scales are critical to developing a computational framework across multiple scales for the rational design of materials with exceptional functionality. mt

Acknowledgments

This material is based upon work supported as part of the HeteroFoaM Center, an Energy Frontier Research Center funded by the U.S. Department of Energy (DOE), Office of Science, Office of Basic Energy Sciences (BES) under Award Number DE-SC0001061. Partial support from the World Class University (WCU) program, UNIST, South Korea, is also acknowledged. The authors wish to thank Prof. Wilson Chiu, Dr. George Nelson, William Harris, and Jeffrey Lombardo at the University of Connecticut for x-ray tomography data used for the simulation shown in Fig. 11c.

REFERENCES

1. Minh, N. Q., and Takahashi, T., *Science and Technology of Ceramic Fuel Cells*. Elsevier: Amsterdam, 1995.
2. Yang, L., *et al.*, *Science* (2009) **326** (5949), 126.
3. Yang, L., *et al.*, *Nat Commu* (2011) **2**, 357.
4. Xia, C. R., *et al.*, *Solid State Ionics* (2002) **149**(1-2), 11.
5. Jiang, S. P., *et al.*, *J Eur Ceram Soc* (2002) **22**(3), 361.
6. Abernathy, H. W., *et al.*, *J Phys Chem C* (2008) **112**(34), 13299.
7. Atkinson, A., *et al.*, *Nature Mater* (2004) **3**(1), 17.
8. Krumpelt, M., *et al.*, *Catal Today* (2002) **77**(1-2), 3.
9. Zha, S., *et al.*, *J Electrochem Soc* (2004) **151**(8), A1128.
10. Cheng, Z., *et al.*, *Energy Environ Sci* (2011) **4**, 4380.
11. Zha, S., *et al.*, *J Electrochem Soc* (2007) **154**(2), B201.
12. Wang, J. -H., and Liu, M., *Electrochem Commun* (2007) **9**(9), 2212.
13. Kreuer, K. D., *Ann Rev Mater Res* (2003) **33**, 333.
14. Malavasi, L., *et al.*, *Chem Soc Rev* (2010) **39**(11), 4370.
15. Kharton, V. V., *et al.*, *Solid State Ionics* (2004) **174** (1-4), 135.
16. Zuo, C. D., *et al.*, *Adv Mater* (2006) **18**(24), 3318.
17. Sun, C. W., *et al.*, *J Solid State Electrochem* (2010) **14**(7), 1125.
18. Niu, Y. J., *et al.*, *J Electrochem Soc* (2011) **158**(2), B132.
19. Chen, D. J., *et al.*, *Electrochem Commun* (2011) **13**(2), 197.
20. Ju, Y. W., *et al.*, *J Electrochem Soc* (2011) **158**(7), B825.
21. Shah, M., *et al.*, *Solid State Ionics* (2011) **187** (1), 64.
22. Lynch, M. E., *et al.*, *Energy Environ Sci* (2011) **4**, 2249.
23. Nie, L. F., *et al.*, *J Power Sources* (2010) **195**(15), 4704.
24. Choi, J., *et al.*, *J Am Ceram Soc* (2011), *in press*.
25. Tao, S., and Irvine, J. T. S., *Nature Mater* (2003) **2**(5), 320.
26. Huang, Y. H., *et al.*, *Science* (2006) **312**(5771), 254.
27. Ruiz-Morales, J. C., *et al.*, *Nature* (2006) **439**(7076), 568.
28. Marina, O. A., *et al.*, *Solid State Ionics* (2002) **149**(1-2), 21.
29. Liu, M., *et al.*, *J Power Sources* (2011) **196**(17), 7277.
30. Lussier, A., *et al.*, *Int J Hydrogen Energy* (2008) **33**(14), 3945.
31. Fleig, J., *Solid State Ionics* (2003) **161**(3-4), 279.
32. Lynch, M. E., and Liu, M. L., *J Power Sources* (2010) **195**(16), 5155.
33. Lynch, M. E., *et al.*, *J Electrochem Soc* (2008) **155**(6), B635.
34. Kawada, T., *et al.*, *J Electrochem Soc* (2002) **149**(7), E252.
35. la O', G. J., *et al.*, *Angew Chem Int Ed* (2010) **49**(31), 5344.
36. Stierle, A., and Molenbroek, A. M., *MRS Bull* (2007) **32**(12), 1001.
37. Choi, Y. M., *et al.*, *ChemPhysChem* (2006) **7**(9), 1957.
38. Pushkarev, V. V., *et al.*, *J Phys Chem B* (2004) **108**(17), 5341.
39. Cheng, Z., *et al.*, *J Phys Chem C* (2007) **111**(49), 17997.
40. Cheng, Z., and Liu, M., *Solid State Ionics* (2007) **178**(13-14), 925.
41. Blinn, K., *et al.*, *J Power Sources* (2011), *submitted*.
42. Eigenbrodt, B. C., *et al.*, *J Phys Chem C* (2011) **115**(6), 2895.
43. Yang, H. Z., *et al.*, *J Phys Chem B* (2006) **110**(35), 17296.
44. Maher, R. C., and Cohen, L. F., *J Phys Chem A* (2008) **112**(7), 1497.
45. Pomfret, M. B., *et al.*, *J Phys Chem C* (2008) **112**(13), 5232.
46. Su, C., *et al.*, *J Power Sources* (2011) **196**(4), 1967.
47. Yoshinaga, M., *et al.*, *J Ceram Soc Jpn* (2011) **119**(1388), 307.
48. Blinn, K. S., *et al.*, *Advances in Solid Oxide Fuel Cells V* (2010) **30**(4), 65.
49. Kudelski, A., *Surf Sci* (2009) **603**(10-12), 1328.
50. Braun, A., *et al.*, *Appl Phys Lett* (2009) **94**(20), 202102.
51. Piper, L. F. J., *et al.*, *J Electrochem Soc* (2011) **158**(2), B99.
52. Yildiz, B., *et al.*, In *Proceedings of the Lucerne Fuel Cell Forum*, Argonne National Laboratory, (2006),
53. Shinoda, K., *et al.*, *Surf Interface Anal* (2010) **42**(10-11), 1650.
54. Liu, D. J., and Almer, J., *Appl Phys Lett* (2009) **94**(22), 224106.
55. Schulz, O., and Martin, M., *Solid State Ionics* (2000) **135**(1-4), 549.
56. Hashimoto, S., *et al.*, *Solid State Ionics* (2011) **186**(1), 37.
57. Kohn, W., and Sham, L. J., *Phys Rev* (1965) **140**, A1133.
58. Choi, Y., *et al.*, *Top Catal* (2007) **46**(3-4), 386.
59. Wang, J. H., *et al.*, In *Quantum Chemical Calculations of Surfaces and Interfaces of Materials* Basiuk, V. A., and Ugliengo, P., (eds.) American Scientific Publishers, Los Angeles, (2008).
60. Huang, P., and Carter, E. A., *Annu Rev Phys Chem* (2008) **59**, 261.
61. Kotomin, E. A., *et al.*, *Phys Chem Chem Phys* (2005) **7**(11), 2346.
62. Choi, Y. M., *et al.*, *Angew Chem Int Ed* (2007) **46**(38), 7214.
63. Choi, Y. M., *et al.*, *J Phys Chem C* (2009) **113**(17), 7290.
64. Chen, H. T., *et al.*, *Langmuir* (2011) **27**(11), 6787.
65. Mastrikov, Y. A., *et al.*, *J Phys Chem C* (2010) **114**(7), 3017.
66. Piskunov, S., *et al.*, *Phys Rev B* (2011) **83**(7), 073402.
67. Choi, Y., *et al.*, *J Power Sources* (2010) **195**(5), 1441.
68. Nikolla, E., *et al.*, *J Am Chem Soc* (2006) **128**(35), 11354.
69. Galea, N. M., *et al.*, *J Phys Chem C* (2007) **111**(39), 14457.
70. Shishkin, M., and Ziegler, T., *J Physl Chem C* (2010) **114**(49), 21411.
71. Wang, J. H., *et al.*, *J Chem Phys* (2007) **127**(21), 214705.
72. Crabtree, G., and Sarrao, J., *Ann Rev Cond Matt Phys* (2011) **2**, 287.
73. Lee, Y. L., *et al.*, *Phys Rev B* (2009) **80**(22), 224101.
74. Lin, H., and Truhlar, D. G., *Theor Chem Acc* (2007) **117**(2), 185.
75. Fleig, J., *Annu Rev Mater Res* (2003) **33**, 361.
76. Adler, S. B., *et al.*, *J Electrochem Soc* (1996) **143**(11), 3554.
77. Virkar, A. V., *et al.*, *Solid State Ionics* (2000) **131**(1-2), 189
78. Sunde, S., *J Electrochem Soc* (1995) **142**(4), L50.
79. Costamagna, P., *et al.*, *Electrochim Acta* (1998) **43**(3-4), 375.
80. Svensson, A. M., *et al.*, *J Electrochem Soc* (1997) **144**(8), 2719.
81. Radhakrishnan, R., *et al.*, *J Electrochem Soc* (2005) **152**(1), A210.
82. Baumann, F. S., *et al.*, *Solid State Ionics* (2006) **177**, 1071.
83. Mebane, D. S., *et al.*, *J Electrochem Soc* (2007) **154**(5), A421.
84. Koep, E., *et al.*, *Electrochem Solid State Lett* (2005) **8**(11), A592.
85. Lankhorst, M. H. R., *et al.*, *Solid State Ionics* (1997) **96**(1-2), 21.
86. Simner, S. P., *et al.*, *Electrochem Solid State Lett* (2006) **9**(10), A478.
87. Singhal, S. C., and Kendall, K., *High Temperature Solid Oxide Fuel Cells: Fundamentals, Design and Applications*. Elsevier: Amsterdam, 2003.
88. Liu, M. L., *J Electrochem Soc* (1998) **145**(1), 142.
89. Lu, Y. X., *et al.*, *J Electrochem Soc* (2009) **156**(4), B513.
90. Wilson, J. R., *et al.*, *Nature Mater* (2006) **5** (7), 541.
91. Gostovic, D., *et al.*, *Electrochem Solid State Lett* (2007) **10** (12), B214.
92. Grew, K. N., *et al.*, *J Electrochem Soc* (2010) **157** (6), B783.
93. Shikazono, N., *et al.*, *J Electrochem Soc* (2010) **157** (5), B665.
94. Joshi, A. S., *et al.*, *J Power Sources* (2007) **164** (2), 631.
95. Joos, J., *et al.*, *ECS Transactions* (2011) **35**, 2357.
96. Lynch, M. E., *et al.*, *in preparation* (2011).
97. Mebane, D. S., and Liu, M., *J Solid State Electrochem* (2006) **10**, 575.
98. Song, M.-K., *et al.*, *Mater Sci Eng R* (2011) **72**, 203.
99. Kroger, N., and Sandhage, K. H., *MRS Bull* (2010) **35**(2), 122.
100. Bao, Z., *et al.*, *Nature* (2007) **446**(7132), 172.